ORIGINAL PAPER

Sunlight-driven organic phase change material-embedded nanofiller for latent heat solar energy storage

M. A. Tony[1,2] · S. A. Mansour[2]

Abstract

Solar energy storage systems hold a key for those seeking for a potential solution of energy issues. The experimental work established in this investigation is based on a composite organic phase change material (PCM) comprised of a technical grade paraffin wax/nanofiller synthesized via ultrasonic dispersion. Various mass fractions of ZnO nanorods synthesized via thermal decomposition technique or silica-coated zinc oxide (SZR) prepared via hydrolysis route were used as a nanofiller embedded in PCM. PCM was applied in a vertical type pipe-in-pipe (PIP) thermal heat storage system connected with a flat plate solar collector where water is used as the heat transfer fluid (HTF). The mass flow rate of the HTF was selected (1.3 g/s) according to the experimental results. The solar intensity data showed the solar collector energy gained was around 170 W, and it was related to the daytime. Results showed the heat transfer rate was affected by the change in the nanofiller type and the mass fraction. Finally, an increase in the heat was gained from 7 to 140 kJ/min with increasing the nanofillers up to a certain limit. Almost 200% system enhancement is achieved for ZSR rather than pristine PW-PCM which makes the system attractive for water heating.

Keywords Phase change material · Energy storage · ZnO nanorods · ZnO/SiO$_2$ nanorods

List of symbols

PCM	Phase change material
PIP	Pipe-in-pipe
PW	Paraffin wax
ZR	Uncoated ZnO nanorods
ZSR	Coated ZnO nanorods with SiO$_2$
SWH	Solar water heating
HTF	Heat transfer fluid
T_a	Air temperature (°C)
T_{ab}	Ambient temperature (°C)
T_ω	Charging temperature of PCM (°C)
T_α	Discharging temperature of PCM (°C)
T_{wic}	Inlet collector water temperature (°C)
T_{woc}	Outlet water temperature from the collector (°C)
T_β	Temperature gained from discharging PCM (°C)
ξ	Collector efficiency (%)
η	Overall efficiency from the PCM storing system (%)
Q_{uc}	Useful heat obtained from collector (W)
Q_β	Rate of useful heat gained from HTF (KJ/min)
Q_{PCM}	Heat gained from PCM (KJ/min)
I_ε	Intensity of solar radiation (W/m^2)
A_c	Area of collector absorber (m^2)
C_p	Specific heat capacity of water 4.18 kJ/kg K (Zelzouli et al. 2012
C_p	Specific heat capacity of paraffin wax 2.1 kJ/kg K (Sharma et al. 2009)
$m^.$	Water mass flow rate (kg/s)
TES	Thermal energy storage
H	Latent heat of fusion of paraffin wax 190 kJ/kg (Sharma et al. 2009)

✉ M. A. Tony
   dr.maha.tony@gmail.com

1 Civil and Environmental Engineering, West Virginia University, Morgantown, WV 26506-6103, USA

2 Advanced Materials/Solar Energy and Environmental Sustainability (AMSEES) Laboratory, Basic Engineering Science Department, Faculty of Engineering, Menoufia University, Shebin El-Kom, Egypt

🖄 Springer

Introduction

Egypt is a country located on the eastern north of the borderline of Africa continent, famously noted for its sunny weather and dry climate over the year especially on the non-coastal regions. Although industry represents a significant proportion of the Egyptian economy, there is a challenge associated with energy crisis (Farahat et al. 2016; Ashour et al. 2014).

As regards a sustainable practical solution and environmental pollution control, solar energy storage in the form of latent heat could reserve as a sustainable energy solution for the electricity shortage, fossil fuels depletion and pollution crises (Sharma et al. 2009; Hajare and Gawali 2015; Chaichan et al. 2015). Sustainable energy plays a vital role not only as a renewable energy source, but also for its rapid distribution (Goldemberga and Coelh 2004). The fundamental purpose of the solar energy storage is to aid energy management by storing the heat in the form of latent heat at periods that sun is abundant and releasing them when it is required as heat and/or hot water in an eco-friendly approach with zero emissions (Kaviarasu and Prakash 2016).

While Egypt is well endowed with sunshine, the renewable solar energy application is still limited in comparison with the global energy need (Tony and Tayeb 2016). To overcome the energy depletion crisis, the Egyptian government vision by 2020 is to substitute about 20% of the total generated energy by electricity with a renewable source (El-Khayat and Ameen 2010).

Although a lot of benefits are associated with the application of solar energy as a sustainable source (Tony et al. 2016), there are downsides such as the high installation cost, inefficiency and inconsistency due to unsteady environmental condition and daytime dependence. Thus, solar energy storage needs to be evolved to improve efficiency of using solar energy (Canbazoglu et al. 2005). In general, solar energy storage is an effective technique to harness solar energy radiation for further uses to cross the unavailability periods of solar radiation to meet energy demand all the times (Sharma et al. 2009). Therefore, in order to overcome the gap between energy needs and supply, latent heat energy storage systems are used to compromise solar energy storage that should retain high storing capacity, be cost efficient with high efficiency and hazard free to the environment (Kaygusuz and Sari 2005; Kaviarasu and Prakash 2016). Solar water heating (SWH) is considered a potential application since it is considered a high-energy storage technique. However, the selection of appropriate storing medium depends on the storing material melting point within the temperature range. Such materials are efficient on storing and releasing a vital amount of heat with

slight temperature variation (Kaygusuz and Sari 2005). Recently, numerous types of organic and inorganic PCM materials were applied such as salt hydrates (Kaygusuz and Sari 2005), paraffin wax (Ho and Gao 2009), fatty acids (Kaviarasu and Prakash 2016) and eutectic materials (Skovajsa et al. 2017). However, the insufficient thermal conductivity and diffusivity make them useful energy storing materials for heating purposes (Kaviarasu and Prakash 2016). Nevertheless, according to the authors' knowledge, there are a few trails in the literature on the application of the so-called PCM as a storing medium on SWH. A pervious investigation conducted by Otanicar and Golden (Otanicar and Golden 2009) compared the conventional and nanofluid SWH technology. In addition, Zeng et al. (2010) examined the thermal performance of PCM for active solar water heating system. Dwivedi et al. (2016) reported that PCM can be successfully integrated with the solar thermal water heating system.

Among the various PCMs types, paraffins are considered the most recommended organic PCM because they are available in low cost, safe, chemically stable, nonreactive, have considerable latent heat of fusion and low vapor pressure in melting, and besides, are thermally efficient although there are a large number of thermal cycles. Conversely, a remarkable low heat transfer rates during the melting/solidification process are as a result of its low thermal conductivity. Therefore, researchers put more efforts into enhancing the thermal conductivity of paraffin PCM such as introducing nanoparticles. For instance, Al_2O_3 nanoparticles (Ho and Gao 2009; Hajare et al. 2014), carbon nanotubes (wang et al. 2009), CuO nanoparticles (Karunamurthy et al. 2012), graphene nanoplatelets (Fang et al. 2013) and TiO_2 and ZnO nanoparticles (Kaviarasu and Prakash 2016) were applied as embedded materials in paraffin-PCM. Although various nano-PCMs have been tested to essentially improve the thermal conductivity, there are limitations in examining their performances on the integrated solar collector applications systems. Such limitations are related to the nanocomposites, i.e., how metal oxide nanoparticles influence the thermal behavior of PCM nanocomposites and what is the possible loading concentration of nanoparticles providing an optimum degree of dispersion throughout PCM, which achieves the unique characteristics of the PCM nanocomposites (Kaviarasu and Prakash 2016). Moreover, the compatibility between nanofiller and the host PCM provides improvement in thermal properties and durability. Many researchers work on surface treatment of nanoparticles by coupling agents to enhance the utilization of nanocomposites (Muller et al. 2017).

This emphasizes the essentials for a new approach in energy storing facilities. Herein, this paper presents the feasibility of two organic paraffin/nanofiller PCM systems derived from synthesized ZnO nanorods and SiO_2-coated

ZnO nanorods for latent heat energy storage. The coating SiO_2 layer could achieve the stability of nanorods in PCM as well as limiting the photodegradation of PCM due to the photoactivity of ZnO nanoparticles (Wen et al. 2011). The heat gained during the charging/discharging processes was used to determine the mechanism of these materials.

Materials and methods

Materials

Commercial paraffin wax (PW) with a melting point around 53 °C and a latent heat of fusion 190 kJ/kg was selected as a base organic PCM material in all experiments. Zinc acetate dihydrate (Winlab, purity 99.999%) used as a precursor for ZnO nanorods. However, tetraethyl orthosilicate, TEOS, assay (GC, area %) ≥ 99.0 area %, purchased from Merck KGaA, and ethanol (Sigma Aldrich ≥ 99.8%) have been used for capping ZnO nanorods by SiO_2.

Synthesis of ZnO nanorods

Thermal decomposition route has been used to synthesize ZnO nanorods. In such route, zinc acetate dihydrate was placed in a covered 50-mL alumina crucible. Thereafter, the crucible was placed in an oven and heated to 350 °C and maintained for 3 h. The heating condition was selected to be sufficient for complete thermal decomposition process of the precursor (Lin and Li 2009). The obtained powder was in dark yellow color. In fact, ZnO is originally off-white powder. However, the heating conditions in the used route of preparation and relative long time of heating in the presence of air could lead to a probable formation of zinc interstitials and oxygen vacancies in the obtained ZnO nanocrystals (Xu et al. 2013; Mallika et al. 2015). So, zinc interstitials should produce lattice defects that switch the color to dark yellow. The final product without surface coating is named ZR referring to non-treated ZnO nanorods.

Silica-coated zinc oxide was prepared according to the typical hydrolysis method for TEOS in the presence of ZnO nanorods as reported by Ramasamy et al. (2014). In this respect, 4 g of as-synthesized ZnO nanorods was dispersed with TEOS (50 wt% to the relevant amount of ZnO). The mixture was sonicated for 10 mim and then stirred overnight to achieve the complete hydrolysis of TEOS. The obtained treated ZnO nanorods were collected by centrifugation and washing with ethanol for four times. The treated sample was dried at 60 °C for 10 h. The obtained surface-coated nanorods with silica were labeled ZSR.

Preparation of PCM nanocomposites

Two types of PCM nanocomposite samples were prepared by mixing treated or non-treated ZnO nanorods with PW. The amount of PW, 15 g, was fixed for all the investigated PCM nanocomposite samples. The concentrations of nanofiller, ZR or ZSR, for each type of nanocomposite were ranged from 0 to 1 wt% from PW. In order to obtain good dispersion of nanorods, the desired amount of PW was melted on hot plate at 60 °C. Thereafter, the desired amount of nanofiller was added, and then, the mixture was exposed to ultrasonic radiation at 60 °C using ultrasonic bath (DAIHAN Wisd model WUC-A03H, 40 kHz).

Characterization techniques

The X-ray diffraction (XRD) measurements for ZR were achieved via XRPhillips X'pert (MPD3040) X-ray diffractometer supported by a monochromatic source CuKa ($k = 1.5406$ A). The XRD measurement was done under step-scan mode, and the registered intensities of the diffracted X-rays were detected every 0.02° over 2 θ range of 20°–80°. Additionally, the morphology of the synthesized treated and non-treated ZnO nanorods, ZSR and ZR, respectively, was checked by high-resolution transmission electron microscopy (HR-TEM, JEM-2100).

Methodology

Description of the experimental facility

The pilot-scale experimental facility testing the PCM was designed and constructed by integrating four parts. The schematic representation of the pilot plant facility is shown in Fig. 4. The first part of the setup is the heating system through a flat plate collector that heats up water, the heat transfer fluid (HTF), which acts as the energy source for the charging PCM installation. Then, the second part is the cooling system, which is based on water HTF in the heat exchanger through the discharging process that in the real facility simulates the energy consumption by the consumers based on the heat exchanger concept. The third part consists of the shell and tube heat exchanger that stores the PCM in the tube of the heat exchanger. Thermal energy is stored in PCM in heat exchanger during the charging process, however releasing it need during the discharging process. The fourth part is a well thermally insulated SWH storage tank that stores the heat released in the solar thermal storing process in the form of hot water. All of the four parts are linked together through rubber tubes piping system transferring the HTF at a certain flow rate. Moreover, the heat loss to the surroundings is minimized using a thermal insulation on the heat exchanger, rubber tubes and the hot water storage tank.

Concept of flat plate solar collector configuration and geographical location

Experiments performed in this study were under the meteorological conditions at Advanced Materials/Solar Energy and Environmental Sustainability (AMSEES) Lab., Faculty of Engineering, Menoufia University, Shebin El-Kom City, Menoufia Governorate, in the north of Egypt. The region is characterized by abundant sunshine and moderate dry climate especially in the summer periods, and the sun shines all over the year. The latitude and longitude of the location are 30°58′N and 31°01′E, respectively, 11 m above sea level (Tony and Tayeb 2011; Farahat et al. 2016). The temperature ranged in the summer season from 28 to 43 °C, and the solar intensity reached 1145 W/m^2.

Solar collector represents the active constituent of the solar heating technique since it gathers the solar radiant energy and then transfers it into heat through the HTF. A typical flat plate collector type is used in this study, which is manufactured from an insulated metal box with a highly transparent glass cover. A steel sheet absorber connected with serpentine form copper tubes acting as the HTF carrier are subjected inside the metal box. The absorbing surface and the copper tubes are painted in a dull black color in order to increase the absorptivity with a collection area of solar radiation of 0.5 m^2, and the mass flow rate is 1.3 g/s. In order to dismiss the heat loss, all sides and the bottom of the collector are thermally insulated. The collector was placed facing the south with a slope angle of 30° with respect to the horizontal line which is suitable for the geographical location. The useful energy gain from this collector controls the temperature rise of the HTF. This collector increases the temperature of the HTF up to 70 °C.

Collector thermal efficiency and energy analysis

The solar collector efficiency ($\xi, \%$) during any period of time is evaluated by the ratio of the amount of useful heat collected through the collector (Q_{uc}, W), [Eq. (2)], to the amount of solar radiation ($I_\varepsilon, W/m^2$) incident on the area of the absorber (A_c, m^2) as given in Eq. (1) (Kurtbash and Durmush 2004; Hematian et al. 2012):

$$\xi = \frac{Q_{uc}}{I_\varepsilon A_c} \times 100 \tag{1}$$

$$Q_{uc} = m^. C_p \left(T_{wic} - T_{woc} \right) \tag{2}$$

where $m^.$ is the rate of water mass flow (kg/s), C_p is the specific heat capacity of water (kJ/kg.K), T_{wic} is the inlet collector water temperature and T_{woc} is the outlet water temperature from the collector.

Description of measurement procedure

The measured variables recorded at time intervals include inlet and outlet HTF temperatures through the collector, ambient temperature, air temperature, PCM temperature, water in the SWH storage tank temperature and the solar radiation.

The intensity of solar radiation incident was measured using an Eppley Black and White solarimeter, model 8–48. This meter was placed adjacent to the collector cover at the same plane.

Thermocouples were positioned evenly; the inlet and outlet water (HTF) temperatures, PCM temperatures and SWH storage tank were measured by two well-insulated thermocouples. All experiments were conducted from 9 am to 5 pm.

Results and discussion

XRD characterization of the nanostructure samples

Figure 1 shows the XRD pattern of the NZRs powder. The registered XRD pattern reveals the formation of ZnO with a wurtzite structure without other ZnO phases or impurity phases.

From the line broadening of the X-ray diffracted lines, the crystallite size (D) of the NZRs was estimated using Williamson–Hall plot (Mote et al. 2012). The equation of the Williamson–Hall approach is given by $\beta_{hkl} \cos \theta = \frac{k\lambda}{D} + 4\varepsilon \sin \theta$, where β_{hkl} represents the full width at half maximum (FWHM) of the peak, k is a constant called the shape factor with the value of 0.94, θ is the Bragg angle and ε is the strain in the sample as a result of crystal
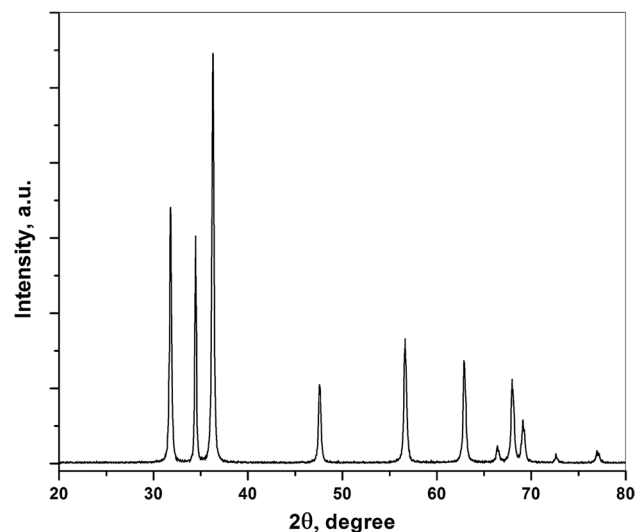

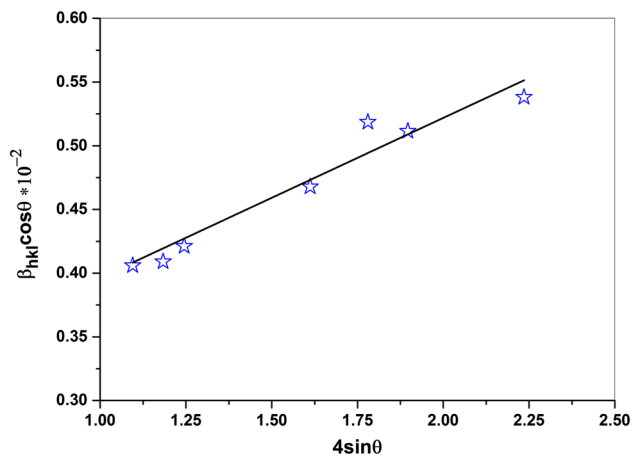**Fig. 1** XRD pattern of the as-synthesized ZnO nanorods

Fig. 2 Williamson–Hall plot for the obtained diffraction data from XRD pattern of the as-synthesized ZnO nanorods

imperfection and/or distortion. Figure 2 shows the relation between $4\sin\theta$ and $\beta_{hkl}\cos\theta$ for the most predominant diffracted peaks. According to the Williamson–Hall and the linear square fitting of such plot, the calculated crystallite size (D) was found to be 53.4 nm, which confirms the nanosize of the investigated sample. Also, the obtained value of a slope, which is equal to ε, was found to be 0.00125. Such positive value of ε is referring to a tensile strain in the sample.

Morphological characterization of the nanostructure samples

Figure 3a shows HR-TEM micrograph of ZR which reveals the successful formation of ZnO nanorods with diameters ranging from 20 to 70 nm. The inset of Fig. 3a shows a single nanorod with high magnification and it has sharply clear surface, whereas Fig. 3b and its inset, for ZSR sample, show the formation of thin layer of SiO_2 as a result of treating ZnO nanorods with SiO_2. Such layer could enhance the dispersion of nanorods in paraffin wax as will be discussed later. On the other hand, the obtained nanorods were loosely aggregated for both samples. In fact, the aggregation zones of nanoparticles can be almost overcome by exposure to ultrasonic radiation (Ramasamy et al. 2014) (Fig. 4).

Solar thermal performance analysis and temperature profile for the flat plate collector

On clear sky condition days, the collector performance investigation was done. Experiments had been conducted during the summer season from May to July 2018. Figure 5 shows different temperature variations throughout the daytime. The ambient temperature (T_{ab}), air temperature (T_a) and the inlet (T_{wic}) and outlet (T_{woc}) temperatures of the HTF subjected to the solar collector at a mass flow rate of
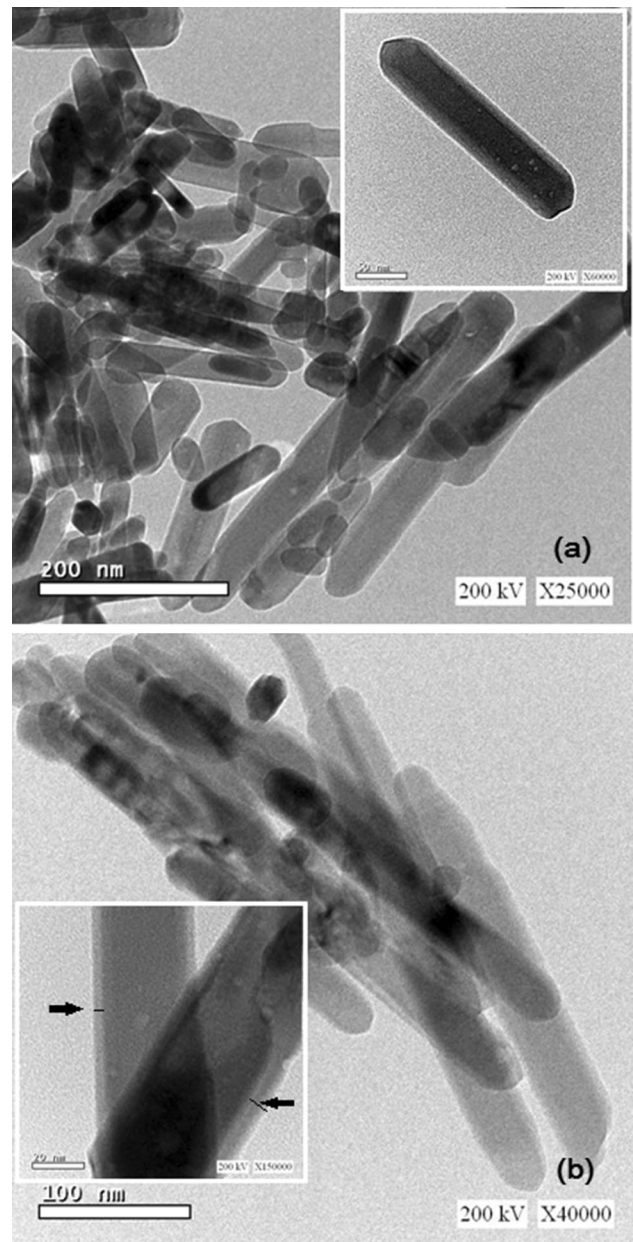

Fig. 3 HR-TEM micrographs of **a** as-synthesized non-treated ZnO nanorods (ZR) and **b** treated, coated by SiO_2, ZnO nanorods (ZSR). The black arrows in the inset of **b** referring to SiO_2 shell and its thickness

1.3g/s were monitored. The measured solar radiation is also shown in Fig. 5. As expected, the solar radiation increased in the morning from 505 W/m^2 to a peak value of 1025 W/m^2 at noon and thereafter began to decrease in the afternoon gradually reaching 500 W/m^2 before the sunset. As shown in the figure, all the temperatures increase to reach their maximum values around the solar noon at 12:00 pm and then, it starts to decrease again later in the afternoon. The temperature ranged from 28 to 34 °C.

Fig. 4 Schematic representation of the pilot-scale experimental PCM-SWH system
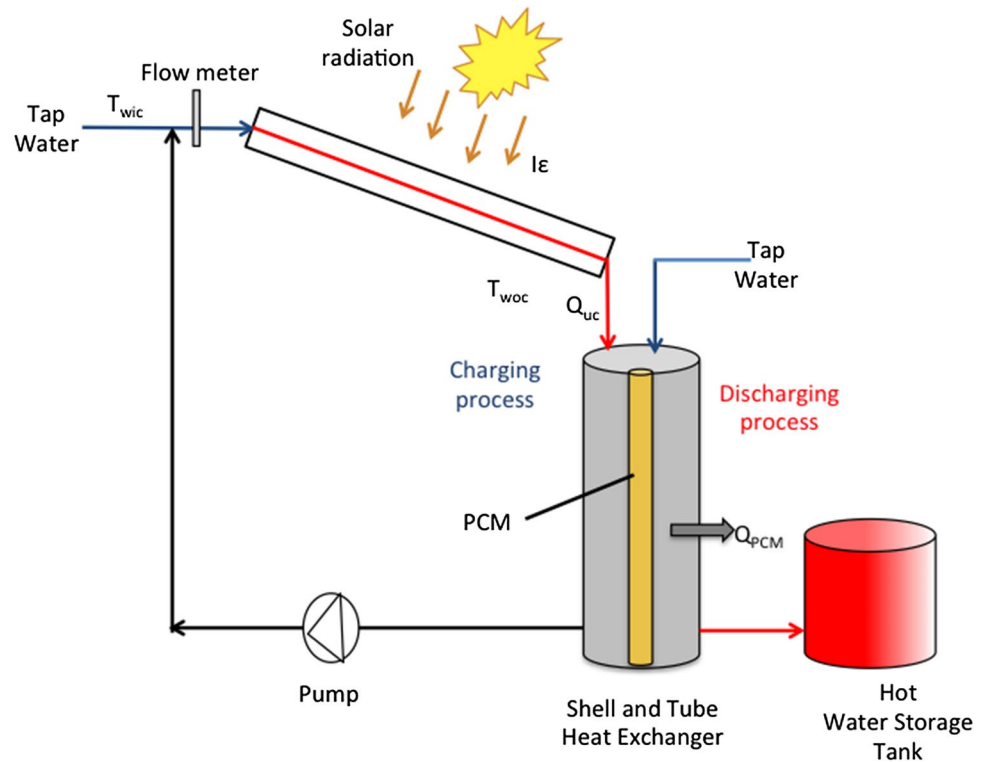

Fig. 5 Thermal analysis of flat plate collector versus time of the day (Egypt, May 6, 2018)
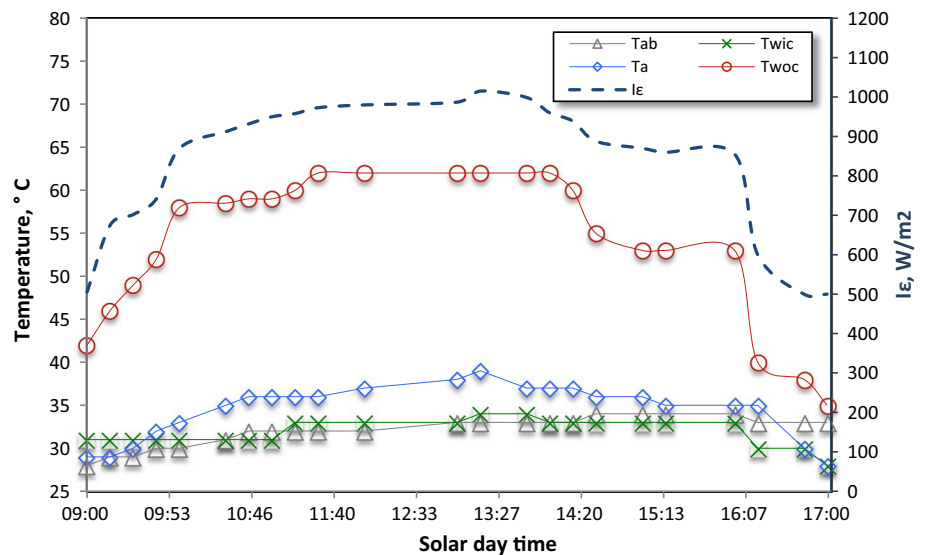

Figure 6a depicts the useful heat gained from the collector variation with daytime, which is obtained from Eq. 2. It is seen from the figure that the amount of heat gained from the collector reached its maximum in the solar noon. As expected, the results reveal that the collector inlet and outlet temperatures increase with the solar radiation (I_ε). Thus, Q_{uc} is increased with increasing temperature as the inlet and outlet temperatures of the HTF increased at a mass flow rate of 0.0013 kg/s. The maximum inlet water temperature reached

its maximum value of 34 °C at the solar noon (13:00 pm), while it decreases again during the afternoon. Furthermore, the corresponding peak of the outlet temperature HTF is reached at 62 °C; thereafter, it decreases again as the solar radiation drops after the solar noon.

According to Fig. 6b, the maximum HTF inlet and outlet temperatures difference of the collector occurred at the time of solar noon (12:30 to 14:30 pm). Thus, the higher collector efficiency calculated from Eq. 1 is gained at the
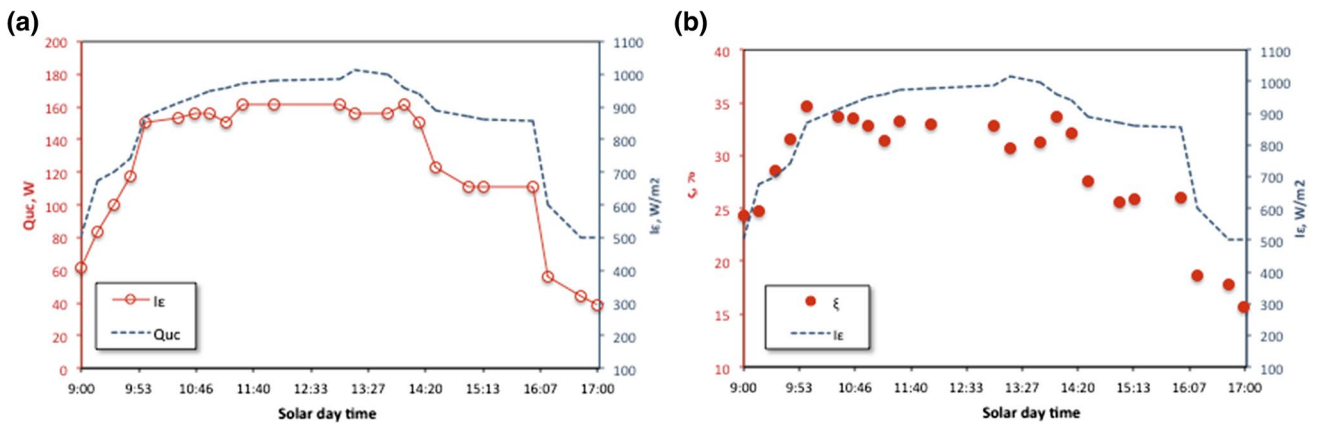
Fig. 6 Energy analysis of the flat plat collector versus time of day and solar intensity, **a** useful energy gained from the collector, **b** variation of collector efficiency
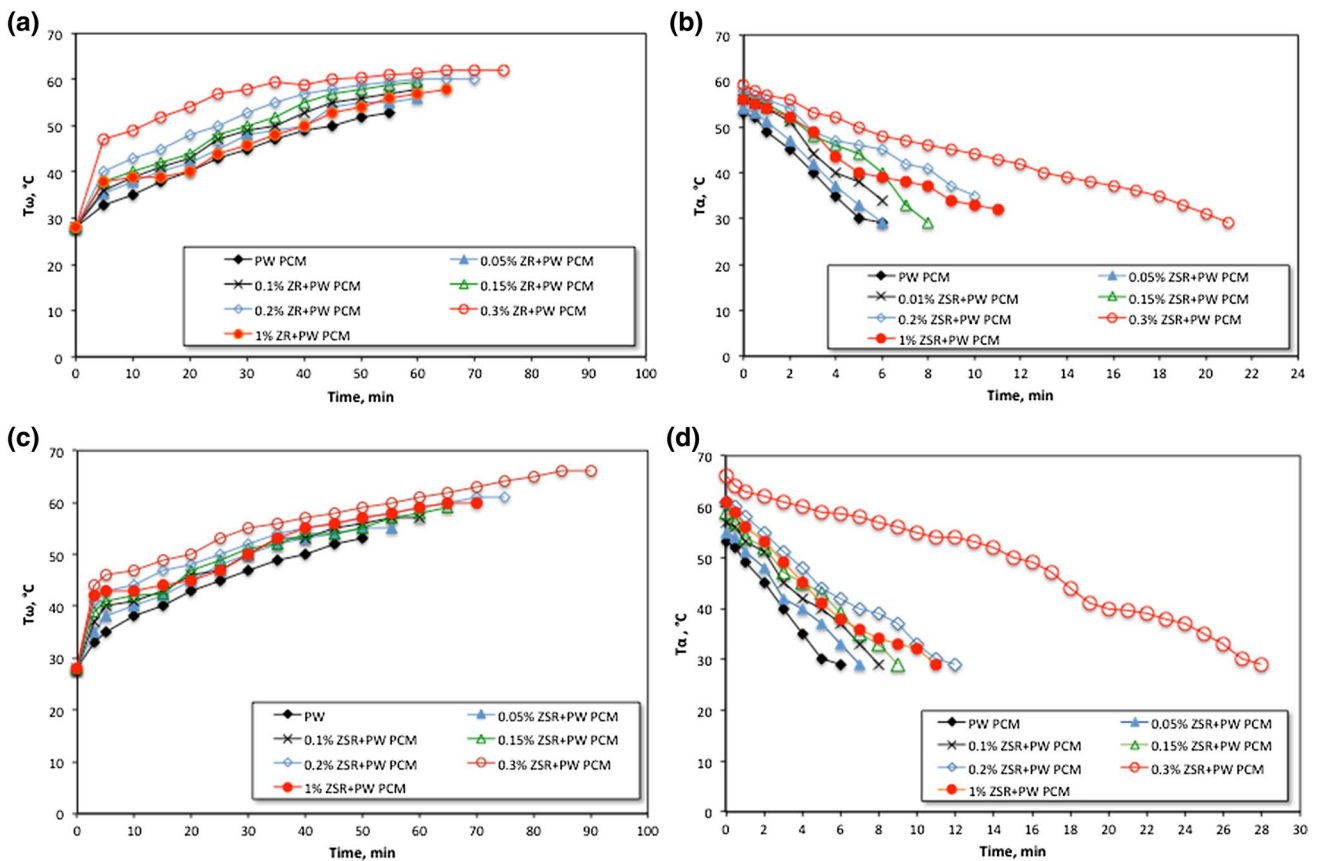

Fig. 7 Thermal behavior of base material and nanoparticle dispersion PCM during **a** charging period of ZR-PCM, **b** discharging period of ZR-PCM, **c** charging period of ZSR-PCM, **d** discharging period of ZSR-PCM

solar noon. Thereafter, even the solar intensity is reduced after the solar noon, the collector efficiency is still high compared to the beginning of the day as the collector's absorber stored the solar energy.

Pilot plant performance of PCM analysis

Charging/discharging cycles

PCM charging (T_ω) and discharging (T_α) temperatures variation cycles are shown in Fig. 7a, b for ZR-PCM, respectively, with respect to time period of charging/discharging at different times. Different ZR-PCMs conditions are compared with the commercial PCM (PW). ZnO nanoparticles at different concentrations (0.05, 0.01, 0.15, 0.2, 0.3 and 1 wt%) are added to the base PW to locate the optimum ZR addition to the PCM. It is noted from Fig. 7a the ZR addition to the PW show a range of melting temperatures. An increase in the temperature was observed by the ZR addition to PW PCM. The most significant system was noted for 0.3% ZR PCM as the temperature of charging reached 62 °C compared to 53 °C for PW PCM without nanoadditives. However, above this amount of ZR, the PCM melting temperature starts to reduce. In particular, according to the literature (Kurtbash and Durmush 2004), the addition of nanoparticles helps to convince a change in the shape of the heat flow of the PCM, thus modifies the value of the melting temperature of the PCM with nanoadditives. Moreover, it is expected that the addition of nanoparticles enhances the latent heat of the PCM. Additionally, the addition of ZnO nanorods controls the photodegradation of PCM (Ramasamy et al. 2014).

The results of discharging cycle of the ZR augmented with that of the pure paraffin PCM are illustrated in Fig. 7b at different ZR compared to PW PCM. As a result of increasing the melting temperature with the addition of ZR, the solidification temperature further increases. Comparing the solidification temperature to that of the pure paraffin, the nanoparticles included in paraffin PCM have a higher solidification temperature, depending on the percentage of nanoparticles mass fraction. The data discerned in Fig. 4b markedly illustrated a relative enhancement of the process when the ZR is together with PW by the increase in the solidification time. Thus, the overall heat stored from the process is increased. The significant enhancement is observed for the 0.3% ZR PCM. However, above 0.3% nanoparticles addition, T_α reduces and thus the process becomes unfavorable. This phenomenon is usually observed experimentally, and this could be illustrated by the fact that excess nanoparticles reduce the stability of the PCM owing to the agglomeration and sedimentation. Therefore, selecting the optimum value of additive nanoparticles into PCM is essential in improving the charging/discharging process performance. This is reported previously in the literature (Teng and Yu 2012; Pise et al. 2013; Chieruzzi et al. 2015). Here, it is worth to mention that the excess of nanofillers in PCM could lead to an increase in dynamic viscosity of PCM which will cause a reduction in heat transfer rate of PCM (Harikrishnan et al. 2014).

Furthermore, comparing Fig. 7c and d with a and b, the results reveal that ZSR-PCM showed a pronounced noticeable effect than ZR-PCM. The treated nanocapsulated PCMs showed a higher charging (T_ω) and discharging (T_α) temperatures than the untreated ZR-PCM as seen in Table 1. The enhanced performance showed an increase of 4 °C for the charging temperature than the untreated ZR. Thus, the nanocapsulated PCMs have a higher thermal stability than the non-capsulated one due to shell-coated ZnO particles. Furthermore, as the amount of nanocapsules mixture increased in the PCM, the heat storage capacity increased. This may be explained by the presence of the coated layer of SiO_2 on ZnO enabling a good dispersion throughout the host paraffin wax. This provides more sites for inorganic nanoparticle materials, which enhances the probability of absorbing heat leading to an increase in the latent heat of fusion of paraffin wax.

This result indicates that the heat storage capacity is related to the amount of the nanocapsules added to the PCM and the optimal addition was found to be 0.3 wt%. This phenomenon is previously stated in the literature (Harikrishnan et al. 2014).

Table 1 Comparison of charging and discharging PCM temperatures of different systems at certain time points

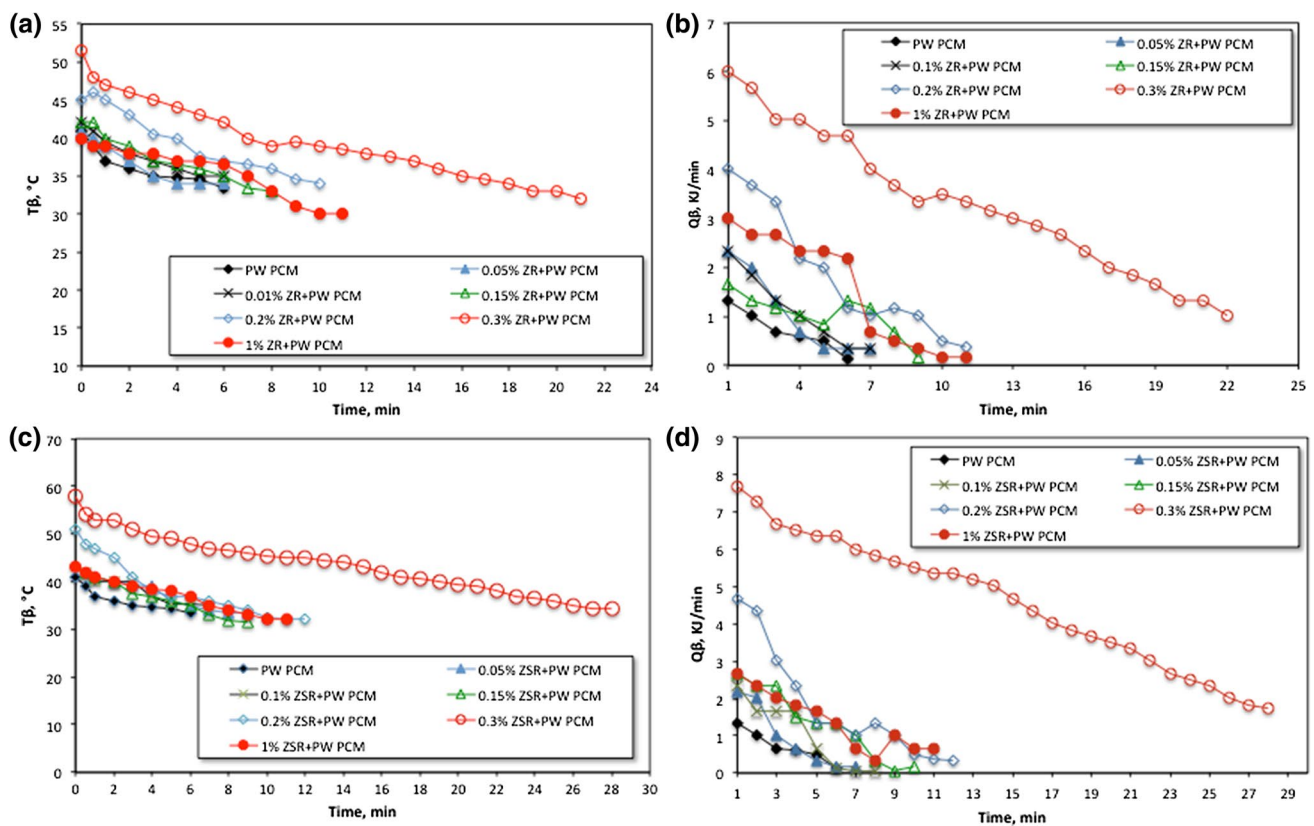| Time (min)	Charging temperature (°C)			Discharging temperature (°C)		
	PW PCM	0.3% ZR + PW PCM	0.3% ZSR + PW PCM	PW PCM	0.3% ZR + PW PCM	0.3% ZSR + PW PCM
0	28	28	28	53	59	66
5	35	46	49	30	50	59
10	38	47	52	28	44	55
20	43	50	57	28	31	40

Fig. 8 The heat storage curves of base material and nanoparticle dispersion PCM: **a** temperature gained from ZR-PCM, **b** heat flow rate during solidification period from ZR-PCM, **c** temperature gained from ZSR-PCM, **d** heat flow rate during solidification period from ZSR-PCM

Heat profile yield

Figure 8 illustrates the temperature gained, T_β, and the amount of heat rate released, Q_β, by the PCM during discharging processes in order to extrapolate from the results the optimal conditions for application in SWH. Consequently, in selecting the optimal additives, it should be considered the heat performance and the range of phase change temperature gained and phase change heat. The experimental results reveal that adding ZnO nanoparticles to paraffin can increase the temperature range and the amount of heat gained, thereby increasing the temperature range of PCM that can be applied to heat storage. Moreover, the ZSR with PW increases the temperature by 10.5 °C that increases the storing up heat compared to the pure paraffin PCM to the optimal 0.3% ZSR PCM (Fig. 5a), maintaining the optimum heat storage capacity. As seen from Fig. 5b, the rate of heat gained from the PCM is increased in the initial period from 1.3 to 6.0 kJ/min for PW and 0.3% ZSR augmented PW PCM. This could be illustrated by the enhancement of nanoparticles which ensures a higher thermal transfer rate that increases with nanoparticle addition especially in the optimal wt% addition value as the specific heat is increased (Fang et al. 2010; Altohamy et al. 2015). Therefore, the

addition of ZnO nanoparticles to paraffin wax to improve heat storage performance has a notable potential for solar water heating application.

The temperature gained and heat rate gained through SWH stored through PCM process are different because the amount of nanocapsules increases from 0.05 to 1 wt% (Fig. 5c, d). However, the maximum heat gained is obtained at the 0.3% ZSR addition to the PCM. The heat gained through the treated ZnO is 7.7 kJ/min compared to 6.0 kJ/min for the untreated ZnO. Thus, this means that the SiO_2 shell-coated ZnO can improve the thermal properties of the microencapsulated paraffin PCM composites because of the synergistic effect between the PW and SiO_2 (Teng and Yu 2012).

Overall heat comparison of TES systems

The overall heat gained from the process is calculated for all PCM systems and compared as illustrated in Fig. 9. The overall heat rate gained by the PCM is the heat transferred by the HTF and is calculated for the whole process by Eq. 2. The pure PW and PW augmented with uncoated nanorods and coated ones PCMs show that the dispersion of nanoadditives to the PW improves the overall heat rate gained from PCM system.

Fig. 9 Comparison of overall heat gained from PCM systems
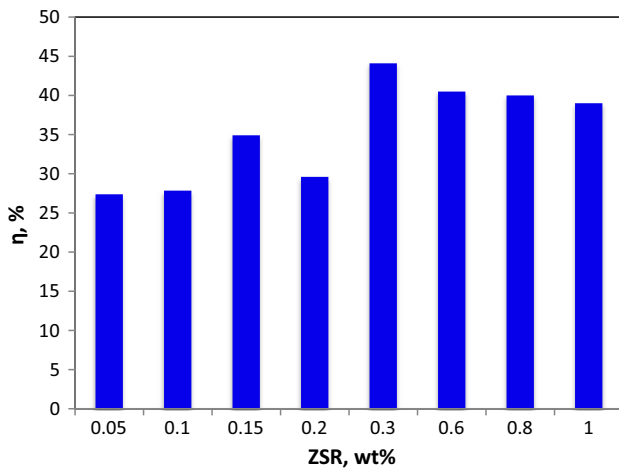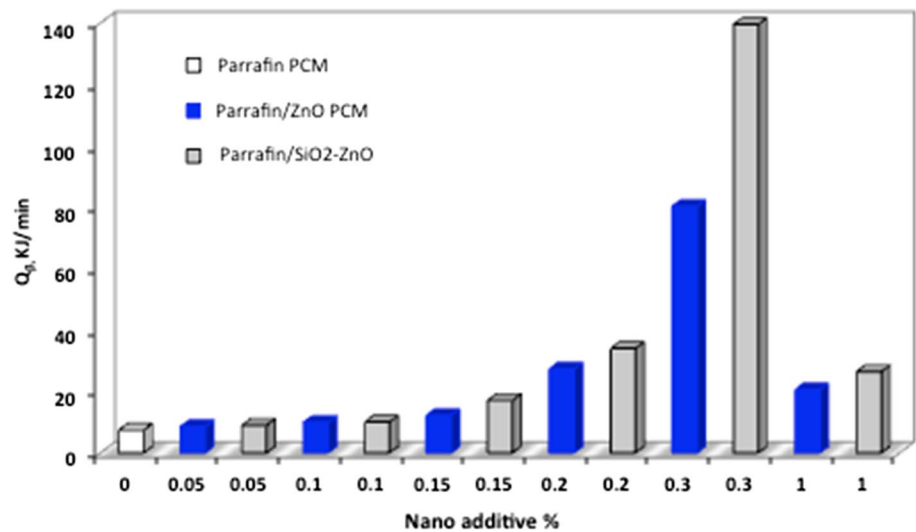

Fig. 10 Comparison of overall efficiency for ZSR PCM system

According to the experimental results, the useful rate of heat gained is greater for composite ZnO nanorods-PW (80.3 kJ/min) than for pristine PW (7.4 kJ/min). Moreover, the capsulated ZnO nanorods–PW-PCM showed a pronounced effect than the heat gained (140 kJ/min) by uncoated ZnO (80.3 kJ/min). In fact, based on this comparison, the significant higher heat rate gained is due to the increase in the heat transfer, due to the higher thermal conductivity of the mixture, and the heat gained rate is more important than the single paraffin. This rate increases proportionately with the weight percentage of the added nanorods. The overall temperature difference during the discharging process and the volume of water stored are higher; thus, the useful heat gained from the PCM process is higher. These results are in agreement with that previously stated in the literature (Kaygusuz and Sari 2005 Altohamy et al. 2015).

From all of the above-obtained results, the use of capsulated ZnO PCM maximizes the storage performance of PCM based on the SWH gained from the investigated system. Thus, the overall storing efficiency of that system at different ZSR additions is compared and illustrated in Fig. 10. Based on the amount of heat gained from HTF (Eq. 2) and the heat gained from the PCM material (Eq. 3), the overall efficiency of the system (η) is calculated in Eq. 4 which is the useful energy gained from the HTF to the heat gained from the PCM (Narayanan et al. 2017).

$$Q_{\mathrm{PCM}} = mC_p\left(T_{\mathrm{PCMi}} - T_{\mathrm{PCMo}}\right) + mH \tag{3}$$

where m is the mass of PCM (kg), C_p is the specific heat capacity of PCM (kJ/kg.K), T_{PCMi} is the inlet PCM temperature, T_{PCMo} is the outlet PCM temperature from the tube of heat exchanger containing PCM and H is the latent heat of fusion of PCM (kJ/kg).

$$\eta = \frac{Q_\beta}{Q_{\mathrm{PCM}}} \times 100 \tag{4}$$

It is clear from Fig. 10 that the efficiency increased with ZSR addition and the maximum efficiency was observed for the 0.3 wt% addition. Thus, these results recommend and confirm that the presence of 0.3% ZSR in the PCM maximizes the efficiency and heat stored from the PCM system.

Conclusion

In this study, the performance of the solar collector efficiency is highly dependent on the solar radiation incident on the collector. The temperature and the useful energy gained

from the collector are highly dependent on that collector efficiency. HTF heated from the collector is used for PCM for energy storage system for application on solar water heating.

The dispersion of two types of nanoparticles in PW was investigated. The results showed that the variation in the heat gained from the process, which is useful for solar water heating, is dependent on the amount of nanoparticles added and the type of dispersed material. Although the dispersion of nanoparticles to the phase change material have a pronounced effect on the system performance, the selection of the type and amount of this nanoadditive are important processes. The coated ZnO nanorods by SiO_2 are more pronounced than the addition of the uncoated one. Moreover, the 0.3% nanoparticle addition to the paraffin PCM maximizes the heat gained from the system.

References

Altohamy AA, Abd Rabbo MF, Sakr RY, Attia AA (2015) Effect of water based Al_2O_3 nanoparticle PCM on cool storage performance. Appl Therm Eng 84:331–338

Ashour EA, Tony MA, Purcell PJ (2014) Use of agriculture-based waste for basic dye sorption from aqueous solution: kinetics and isotherm studies. Am J Chem Eng 2(6):92–98

Canbazoglu S, Sahinaslan A, Ekmekyapar A, Akosy YG, Akarsu F (2005) Enhancement of solar thermal energy storage performance using sodium thiosulfate pentahydrate of a conventional solar water heating system. Energy Build 37:235–242

Chaichan MT, Kamel SH, Al-Ajeely AN (2015) Thermal conductivity enhancement by using nano-material in phase change material for latent heat thermal energy storage systems. Saussurea 5(6):48–55

Chieruzzi M, Miliozzi A, Crescenzi T, Torre L, Kenny JM (2015) A new phase change material based on potassium nitrate with silica and alumina nanoparticles for thermal energy storage. Nanoscale Res Lett 10:273

Dwivedi VK, Tiwari P, Tiwari S (2016) Importance of phase change material (pcm) in solar thermal applications: a review. In: International conference on emerging trends in electrical, electronics and sustainable energy systems (ICETEESES–16), March 11–12

El-Khayat MM, Ameen EE (2010) Renewable energy in egypt—challenges and prospects. In: Thermal Issues in Emerging Technologies, Cairo, Egypt, December 19–22

Fang G, Chen Z, Li H (2010) Synthesis and properties of microencapsulated paraffin composites with SiO_2 shell as thermal energy storage materials. Chem Eng J 163:154–159

Fang X, Fan L, Ding Q, Wang X, Yao XL, Hou JF, Yu Z, Chen G, Hu Y, Cen K (2013) Increased thermal conductivity of eicosane-based composite phase change materials in the presence of graphene nanoplatelets. Energy Fuels 27(7):4041–4047

Farahat MA, Mousa MM, Mahmoud NH (2016) Solar distiller with flat plate collector and thermal storage. In: 17th international conference on applied mechanics and mechanical engineering, Military Technical College, Cairo, Egypt, pp 19–21

Goldemberga J, Coelh ST (2004) Renewable energy—traditional biomass vs. modern biomass. Energy Policy 32:711–714

Hajare VS, Gawali BS (2015) Experimental study of latent heat storage system using nano-mixed phase change material. Int J Eng Technol Manag Appl Sci 3(8):37–44

Hajare VS, Narode AR, Gawali BS, Bamane SR (2014) Experimental investigation of enhancement in heat transfer using nano-mixed PCM. Int J Eng Res Technol 3(11):843–848

Harikrishnan S, Deenadhayalan M, Kalaiselvam S (2014) Experimental investigation of solidification and melting characteristics of composite PCMs for building heating application. Energy Convers Manage 86:864–872

Hematian A, Ajabshirchi Y, Behfar H, Ghahramani H (2012) Designing, construction and analysis of speed control system of the fan with PV feeding source in an air solar collector. Mod Appl Sci 6(1):136–144

Ho CJ, Gao JY (2009) Preparation and thermophysical properties of nanoparticle-in-paraffin emulsion as phase change material. Int Commun Heat Mass Transf 36:467–470

Karunamurthy K, Murugumohan K, Suresh S (2012) Use of Cuo nanomaterial for the improvement of thermal conductivity and performance of low temperature energy storage system of solar pond. Digest J Nanomater Biostruct 7(4):1833–1841

Kaviarasu C, Prakash D (2016) Review on phase change materials with nanoparticle in engineering applications. J Eng Sci Technol Rev 9(4):26–386

Kaygusuz K, Sari A (2005) Thermal energy storage system using a technical grade paraffin wax as latent heat energy storage material. Energy Sources 27:1535–1546

Kurtbash I, Durmush A (2004) Efficiency and exergy analysis of a new solar air heater. Renew Energy 29(9):1489–1501

Lin C, Li Y (2009) Synthesis of ZnO nanowires by thermal decomposition of zinc acetate dihydrate. Mater Chem Phys 113:334–337

Mallika AN, Reddy AR, Reddy KV (2015) Annealing effects on the structural and optical properties of ZnO nanoparticles with PVA and CA as chelating agents. J Adv Ceram 4(2):123–129

Mote VD, Purushotham Y, Dole BN (2102) Williamson-Hall analysis in estimation of lattice strain in nanometer-sized ZnO particles. J Theor Appl Phys 6(1):6–14. https://doi.org/10.1186/2251-7235-6-6

Muller K, Bugnicourt E, Latorre M, Jorda M, Sanz YE, Lagaron JM, Miesbauer O, Bianchin A, Hankin S, Bolz U, Perez G, Jesdinszki M, Lindner M, Scheuerer Z, Castello S, Schmid M (2017) Review on the processing and properties of polymer nanocomposites and nanocoatings and their applications in the packaging automotive and solar energy fields. Nanomaterials 7(4):74

Narayanan S, Kardam SA, Kumar V, Bhardwaj N, Madhwal D, Shukla P, Kumar A, Verma A, Jain VK (2017) Development of sunlight-driven eutectic phase change material nanocomposite for applications in solar water heating. Resour Eff Technol 3(3):272–279

Otanicar TP, Golden JS (2009) Comparative environmental and economic analysis of conventional and nanofluid solar hot water technologies. Environ Sci Technol 43:6082–6087

Pise AT, Waghmare AV, Talandage VG (2013) Heat transfer enhancement by using nanomaterial in phase change material for latent heat thermal energy storage system. Asian J Eng Appl Technol 2(2):52–57

Ramasamy M, Das M, An SN, Yi DK (2014) Role of surface modification in zinc oxide nanoparticles and its toxicity assessment toward human dermal fibroblast cells. Int J Nanomed 9:3707–3718

Sharma A, Tyagi VV, Chen CR, Buddhi D (2009) Review on thermal energy storage with phase change materials and applications. Renew Sustain Energy Rev 13:318–345

Skovajsa J, Kolacek M, Zalesak M (2017) Phase change material based accumulation panels in combination with renewable energy sources and thermoelectric cooling. Energies 10:152

Teng T, Yu C (2012) Characteristics of phase-change materials containing oxide nano-additives for thermal storage. Nanoscale Res Lett 7:611

Tony MA, Tayeb A (2011) The use of solar energy in a low-cost drying system for solid waste management: concept, design and performance analysis. In: Eurasia waste management symposium, 14–16 November

Tony MA, Tayeb A (2016) Response surface regression model in optimization of alum sludge drying facility: solar-fenton's reagent dewatering. Int J Chem Eng Appl 7(5):331–335

Tony MA, Tayeb A, Zhao YQ (2016) An alternative arrangement for the alum sludge management: minimising waste with low-cost solar techniques. Am J Chem Eng 4(2):30–37

Wang J, Xie H, Xin Z, Li Y, Chen L (2009) Thermal properties of paraffin based composites containing multi-walled carbon nanotubes. Thermochim Acta 488:39–44

Wen BF, Wang X, Xu Y, Zhang D, Yang M (2011) The effect of encapsulation of nano zinc oxide with silica on the UV resistance of polypropylene. Polym Plast Technol Eng 50:1375–1382

Xu J, Shi S, Zhang X (2013) Structural and optical properties of (Al, K)-co-doped ZnO thin films deposited by a sol–gel technique. Mater Sci Semicond Process 16:732–737

Zelzouli K, Guizani A, Sebai R, Kerkeni C (2012) Solar thermal systems performances versus flat plate solar collectors connected in series. Engineering 4:881–893

Zeng RX, Wang W, Xiao Y, Zhang Q, Di H (2010) Thermal performance of phase change material energy storage floor for active solar water-heating system. Front Energy Power Eng Chin 4(2):185–191